PASJ: Publ. Astron. Soc. Japan **60**, 1013–1021, 2008 October 25

VLBI Astrometry of AGB Variables with VERA — A Semiregular Variable S Crateris —

Akiharu NAKAGAWA,[1] Miyuki TSUSHIMA,[2] Kazuma ANDO,[2] Takeshi BUSHIMATA,[3,4] Yoon Kyung CHOI,[5] Tomoya HIROTA,[1,6] Mareki HONMA,[3,6] Hiroshi IMAI,[1] Kenzaburo IWADATE,[7] Takaaki JIKE,[7] Seiji KAMENO,[1] Osamu KAMEYA,[5,7] Ryuichi KAMOHARA,[3] Yukitoshi KAN-YA,[8] Noriyuki KAWAGUCHI,[3] Masachika KIJIMA,[5] Mi Kyoung KIM,[5] Hideyuki KOBAYASHI,[3,4,5,7] Seisuke KUJI,[7] Tomoharu KURAYAMA,[3] Toshihisa MAEDA,[2] Seiji MANABE,[6,7] Kenta MARUYAMA,[2] Makoto MATSUI,[2] Naoko MATSUMOTO,[2] Takeshi MIYAJI,[3,4] Takumi NAGAYAMA,[2] Kayoko NAKAMURA,[2] Daisuke NYU,[2] Chung Sik OH,[3,6] Toshihiro OMODAKA,[1] Tomoaki OYAMA,[3] Nicolas PRADEL,[3] Satoshi SAKAI,[7] Tetsuo SASAO,[9,10] Katsuhisa SATO,[7] Mayumi SATO,[7] Katsunori M. SHIBATA,[3,4,6] Hiroshi SUDA,[7] Yoshiaki TAMURA,[6,7] Kousuke UEDA,[2] Yuji UENO,[7] and Kazuyoshi YAMASHITA[6]

[1]*Faculty of Science, Kagoshima University, 1-21-35 Korimoto, Kagoshima, Kagoshima 890-0065*
nakagawa@astro.sci.kagoshima-u.ac.jp
[2]*Graduate School of Science and Engineering, Kagoshima University, 1-21-35 Korimoto, Kagoshima, Kagoshima 890-0065*
[3]*Mizusawa VERA Observatory, National Astronomical Observatory of Japan, 2-21-1 Osawa, Mitaka, Tokyo 181-8588*
[4]*Space VLBI Project, National Astronomical Observatory of Japan, 2-21-1 Osawa, Mitaka, Tokyo 181-8588*
[5]*Department of Astronomy, Graduate School of Science, The University of Tokyo, 7-3-1 Hongo, Bunkyo-ku, Tokyo 113-0033*
[6]*Department of Astronomical Sciences, Graduate University for Advanced Studies, 2-21-1 Osawa, Mitaka, Tokyo 181-8588*
[7]*Mizusawa VERA Observatory, National Astronomical Observatory of Japan, 2-12 Hoshi-ga-oka, Mizusawa-ku, Oshu-shi, Iwate 023-0861*
[8]*Department of Astronomy, Yonsei University, 134 Shinchong-dong, Seodaemun-gu, Seoul 120-749, Republic of Korea*
[9]*Department of Space Survey and Information Technology, Ajou University, Suwon 443-749, Republic of Korea*
[10]*Korean VLBI Network, Korea Astronomy and Space Science Institute, P.O.Box 88, Yonsei University, 134 Shinchon-dong, Seodaemun-gu, Seoul 120-749, Republic of Korea*

(Received 2008 January 23; accepted 2008 August 5)

Abstract

We present a distance measurement for the semiregular variable S Crateris (S Crt) based on its annual parallax. With the unique dual beam system of the VLBI Exploration for Radio Astrometry (VERA) telescopes, we measured the absolute proper motion of a water maser spot associated with S Crt, referred to the quasar J1147−0724 located at an angular separation of 1.°23. In observations spanning nearly two years, we detected the maser spot at an LSR velocity of 34.7 km s^{-1}, for which we measured an annual parallax of 2.33 ± 0.13 mas, corresponding to a distance of 430^{+25}_{-23} pc. This measurement has an accuracy one order of magnitude better than the parallax measurements of HIPPARCOS. The angular distribution and three-dimensional velocity field of maser spots indicate a bipolar outflow with the flow axis along the northeast–southwest direction. Using the distance and photospheric temperature, we estimated the stellar radius of S Crt and compared it with those of Mira variables.

Key words: astrometry — masers (H_2O) — stars: AGB and post-AGB — stars: individual (S Crateris) — stars: variables: other

1. Introduction

Very Long Baseline Interferometry (VLBI) is a powerful technique for obtaining the positions of celestial objects with milliarcsecond (mas) level accuracy. The VLBI Exploration of Radio Astrometry (VERA) is a Japanese VLBI array dedicated to phase referencing VLBI (Kobayashi et al. 2003). VERA consists of four 20 m diameter antennas at Mizusawa, Ogasawara, Iriki, and Ishigaki-jima (see figure 1 of Petrov et al. 2007). To overcome phase fluctuations and the limited integration time in conventional fast-switching VLBI, VERA has a dual-beam system that allows simultaneous observations of target and reference sources separated by 0.°3 to 2.°2. This advanced capability of VERA can be used to measure annual parallaxes and proper motions of masers with a 10 micro arcsecond (μas) level accuracy.

An annual parallax gives a simple geometrical measure of the distance, free from the complex assumptions required in other distance estimators. Studies of Asymptotic Giant Branch (AGB) stars by Whitelock, Feast, and van Leeuwen (2008), Kurayama, Sasao, and Kobayashi (2005), and Vlemmings et al. (2003) are based on the annual parallax derived from VLBI observations, and have demonstrated the the ability of VLBI astrometry. More recently, successful measurements of distances and proper motions with VERA have been reported (Hirota et al. 2007; Honma et al. 2007; Imai et al. 2007; Hirota et al. 2008; Sato et al. 2007). In the present paper, we report on the observations of S Crateris (S Cri), while concentrating

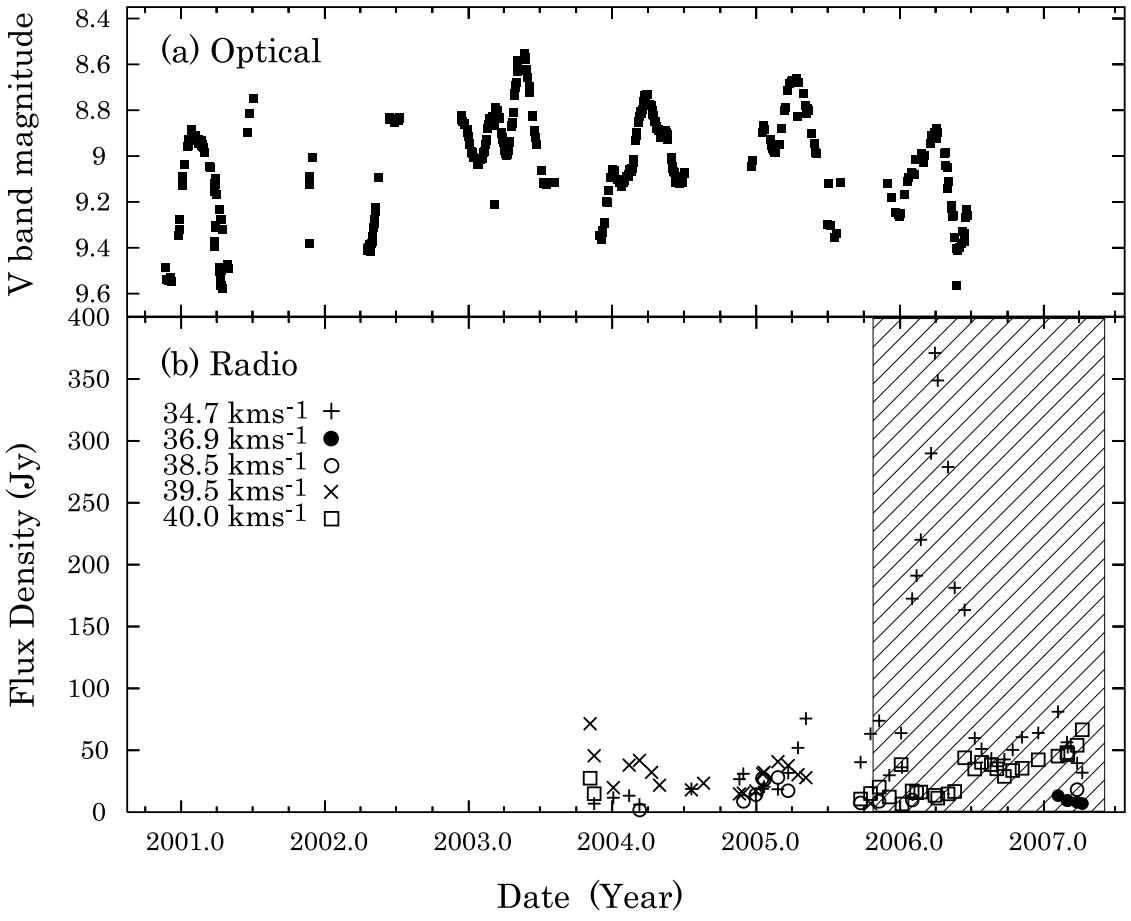

Fig. 1. Light curves of S Crt. (a) Optical light curve at the V band provided by the ASAS (Pojmański 1997). (b) Water maser light curve at 22 GHz obtained with the single-dish monitoring program with VERA (Shintani et al. 2008). Peak flux densities of major velocity components are presented with different symbols. The symbols of "+", "●", "○", "×", and "□" indicate the peak fluxes of the individual components at the LSR velocities of 34.7, 36.9, 38.5, 39.5, and 40.0 km s^{-1}, respectively. There were no available data before the year of 2003.8. The hatched area indicates the period of the present VLBI monitoring observations.

on the distance measurement. S Crt (IRAS 11501−0719, IRC −10259, AFGL 4830S) is an AGB star, with a pulsation period of 155 d (Benson et al. 1990). S Crt has a variability type of SRb in the General Catalog of Variable Stars (Antipin et al. 2005). The apparent magnitude at the K band is 0.786 ± 0.314 mag (R. M. Cutri et al. 2003).[1] The optical light curve in the V band is presented in figure 1a, exhibiting an ~ 0.8 mag variation.

The distance to S Crt has been measured in various ways. Bowers and Johnston (1994) and Patel, Joseph, and Ganesan (1992) determined the distance to be 420 pc and 285 pc, respectively, using the period–luminosity (PL) relation of Mira variables. Perryman et al. (1997) used HIPPARCOS data to measure a parallax of 2.04 ± 1.31 mas, corresponding to a distance of 490 pc, but with an large uncertainty. Recently, the new HIPPARCOS catalog (van Leeuwen 2007) gives a parallax of 1.27 ± 0.92 mas, corresponding to a distance of 787 pc. VERA offers the potential to determine the parallax with a better accuracy, so that the inconsistencies in these distance measurements can be resolved.

[1] The IRSA 2MASS All-Sky Point Source Catalog, NASA/IPAC Infrared Science Archive ⟨http://irsa.ipac.caltech.edu/applications/Gator/⟩.

The observations and data reduction are described in section 2. In section 3, we present the absolute positions and internal motions of maser spots. The annual parallax of S Crt is presented and converted to the absolute distance in this section. Finally, in section 4, we examine the properties of S Crt in the context of the new distance measurement.

2. Observations and Data Reduction

2.1. *Observations*

We conducted a series of monthly VLBI observations from 2005 October to 2007 May with VERA. The duration of each observation was typically 8.5 hr, yielding a net integration time of 5 to 6 hr. The typical synthesized beam size (FWHM) was 1.5 mas × 0.8 mas with a position angle (P.A.) of −30°. To obtain the positions of maser spots in S Crt, the quasar J1147−0724 was simultaneously observed as the position reference. The J2000 a priori coordinates of two sources are $(\alpha,\ \delta) = (11^{\rm h}52^{\rm m}45\overset{\rm s}{.}0981,\ -07°35'48\overset{''}{.}072)$ for S Crt, and $(11^{\rm h}47^{\rm m}51\overset{\rm s}{.}554035,\ -07°24'41\overset{''}{.}14109)$ for J1147−0724. J1147−0724 is classified as a "candidate" source in the catalog of the International Celestial Reference Frame (ICRF), and

Table 1. Observations.

ID	Date	Year/DOY
1*	2005 October 19	2005/292
2*	2005 December 3	2005/337
3*	2006 January 5	2006/005
4*	2006 February 11	2006/042
5*	2006 March 10	2006/069
6*	2006 May 9	2006/129
7*	2006 November 13	2006/317
8*	2006 December 11	2006/345
9	2007 January 13	2007/013
10*	2007 February 21	2007/052
11	2007 April 06	2007/096
12	2007 May 10	2007/130

* The observations used in the estimation of the annual parallax.

its position errors are 270 μas and 290 μas in RA and Dec, respectively (Ma et al. 1998). The separation and P.A. of these sources are 1.°23 and $-80°$.

From a total of 17 observations, we used 12 observations in the present study. The observation in 2005 November was not used because the Ishigaki-jima antenna did not participate. Bad weather conditions in four observations held between August and October in 2006 resulted in much higher system noise temperatures ($\geq$ 500 K) at some of the stations. The shorter integration times and unsolved phase fluctuations in these four observations degraded the image qualities of S Crt in both self-calibration and phase reference analyses.

The observation status is summarized in table 1, which is organized as follows: Column (1) — The ID number of epoch. The number with an asterisk "*" indicates that the observation was used in the estimation of the annual parallax. Column (2) — Date of the observation. Column (3) — The year and day of the year (DOY). In the observations in 2007/013, 2007/096, and 2007/130, the phase referenced images are scattered into several components, while the self-calibrated images resulted in a single bright component, clearly indicating that the atmospheric conditions on these days prohibited successful 22 GHz phase referencing. We did not use these three observations for the parallax estimation. In parallel with the VLBI program, we have monitored S Crt with single-dish observations at the Iriki station since 2003 September with a typical interval of one month (see also Shintani et al. 2008).

A data recording rate of 1024 Mbps was adopted with the VERA DIR2000 recording system, which yields a total receivable bandwidth of 256 MHz with 2-bit digitization. The 256 MHz bandwidth data of left-hand circular polarization were divided into 16 IF channels of 16 MHz band width, one of which was used to receive the maser emission; the others were used to receive the continuum emission from J1147−0724. A cross-correlation was carried out with the Mitaka FX correlator (Shibata et al. 1998) at the National Astronomical Observatory of Japan (NAOJ). In most observations, the IF channel assigned to the water maser was divided into 512 spectral channels, yielding a frequency spacing of 31.25 kHz, corresponding to a velocity resolution of 0.42 km s^{-1}. The observations in 2006/069 and 2006/129 provided a two-times higher frequency resolution than other observations, yielding a velocity resolution of 0.21 km s^{-1}. For the data of J1147−0724, the IF channels were divided into 64 spectral channels in all observations.

2.2. *Calibration and Imaging*

We used the Astronomical Imaging Package Software (AIPS) developed at the National Radio Astronomical Observatory (NRAO) for data reduction. An amplitude calibration was achieved using the system noise temperatures and gains logged during the observations at each station. In the fringe search process of the reference source J1147−0724, we used the task FRING with a typical integration time of 2 min, with solutions of the fringe phases, group delays, and delay rates obtained every 30 s. Using the task TACOP, these solutions were transfered to the data of S Crt in order to calibrate the visibility data. Phase and amplitude solutions obtained from self-calibration of the J1147−0724 were also transferred to the S Crt data.

Since the delay-tracking models used to estimate a priori delays in the Mitaka FX correlator were not accurate enough for astrometry with VERA, we have applied better estimates calculated with the CALC3/MSOLV software package (Jike et al. 2005). Manabe, Yokoyama, and Sakai (1991) gave a brief description of this package in a report to the International Earth Rotation Service (IERS). CALC3 has slight differences in the physical models than those adopted in CALC, which was developed by a research group at NASA Goddard Space Flight Center (GSFC). Comparing the two a priori values from the Mitaka FX correlator and the CALC3/MSOLV package, we obtained the difference between the two estimates, and then applied them to the visibility data using the tasks TBIN and CLCAL in AIPS. We note that the zenith excess path lengths due to the wet atmosphere measured by the global positioning system (GPS) at each station are considered in the CALC3/MSOLV package.

We estimated the residual atmospheric zenith delay offset using the method described in Honma et al. (2007). This correction was applied to one of the four stations of VERA where the coherence of the phase-referenced image was maximized. Typically, the offsets were found to be within $\pm$ 3 cm.

The instrumental delay caused by the difference between two signal paths was estimated using an artificial noise source (Kawaguchi et al. 2000). These delays were then loaded into AIPS and applied in the same manner as the delay tracking model correction. For each observation, we fitted a two-dimensional Gaussian model to the brightness distribution to find the position of the maser spot. We then used these to derive the annual parallax and linear proper motions (μ_X, μ_Y).

In the single-beam VLBI imaging of S Crt, group delays solved with 3C 279 were applied, then fringe-fitting was done using the brightest emission showing an LSR velocity of 34.7 km s^{-1}. Thus, the relative positions of all maser spots in self-calibrated images were determined with respect to this reference spot. For each velocity channel, the position of the spot is defined as the brightness peak of the image. To estimate the relative motion of each spot, a linear least-squares analysis was applied to the spot seen at the same velocity channel during at least two continuous observations. A signal-to-noise ratio of 10 was adopted as the detection criterion in

the self-calibrated images. The rms noise of the self-calibrated images was typically 90 mJy beam^{-1}. On the other hand, the rms noise of the phase-referenced images was typically 700 mJy beam^{-1}, about one order of magnitude larger than that of self-calibrated images. Due to a limited phase coherence, the phase-referenced images have a limited signal-to-noise (30 vs. 307 in the self-calibrated images).

3. Results

3.1. Annual Parallax and Distance

In figure 2, cross-power spectra of S Crt from 2005/069 (top) and 2006/292 (bottom) on the Mizusawa–Iriki baseline are presented. The time variation of the flux densities with the total power spectrum are presented in figure 1b with an indication of each LSR velocity. The 34.7 km s^{-1} spot underwent a radio flare (e.g., Shimoikura et al. 2005). This flare started in 2006 February, and reached a maximum of 371 Jy in March 31 (2006/090), and then decreased to 60 Jy in July. During the flare, this spot did not show any structural change. The cross-power spectrum at the same time showed a significantly weaker ($\simeq$ 30%) flux density than that of the total power spectrum, indicating that some of the flared emission was resolved on the VERA baselines.

In figure 3, we present the positions of the maser spot at an LSR velocity of 34.7 km s^{-1} relative to the phase tracking center. Throughout the present VLBI observations, this maser spot was bright enough to be detected on all baselines in phase referencing analyses. The proper motion was clearly modulated by the parallax. Based on a least-squares fitting analysis, the parallax was determined to be 2.33 ± 0.13 mas, which corresponds to a distance of 430^{+25}_{-23} pc. Here, we adopted position errors of each measurement that were obtained as the root sum squares of three error factors; the details are given in subsection 4.1.

To estimate the parallax, we adopted a very small number of assumptions: the maser spot is moving on a linear trajectory with respect to the star, i.e., there is no acceleration, and the reference source is fixed on the sky, i.e., no motions due to a core shift or jet features. From the fitting results, the linear proper motions of the reference spot (μ_X, μ_Y) were obtained to be (μ_X, μ_Y) = (-1.56 ± 0.22 mas yr^{-1}, -5.16 ± 0.22 mas yr^{-1}). This motion is a combination of the proper motion of the S Crt system and the internal motion of the maser spot in the system. Considering the offset of the reference spot from the phase tracking center ($\Delta\alpha$, $\Delta\delta$) = (-8.49 mas, -23.81 mas), the J2000.0 absolute coordinates of this spot in 2005/292 were obtained to be (α, δ) = ($11^{\rm h}52^{\rm m}44.^{\rm s}96969$, $-07°35'48.''0958$). This is the position as referenced to the position of J1147−0742, and in relative offset to the original phase tracking centre. The uncertainty of this position is estimated to be $\sim 400\,\mu$as, based on the errors in our phase referencing analysis (detailed in subsection 4.1) and the ICRF position of J1147−0724.

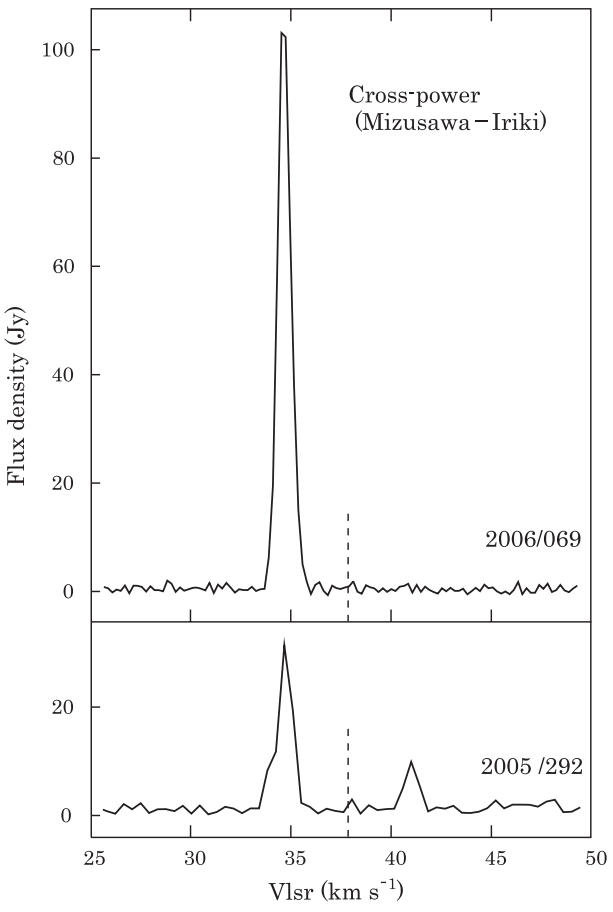

Fig. 2. Cross-power spectra of the S Crt water masers observed with the Mizusawa–Iriki baseline on 2005/069 (top) and 2006/292 (bottom). The stellar velocity of 37.85 km s^{-1} is indicated by the vertical dashed line in the spectra. The blue-shifted component with respect to the stellar velocity has been brighter than the red-shifted one in the majority of our observations.

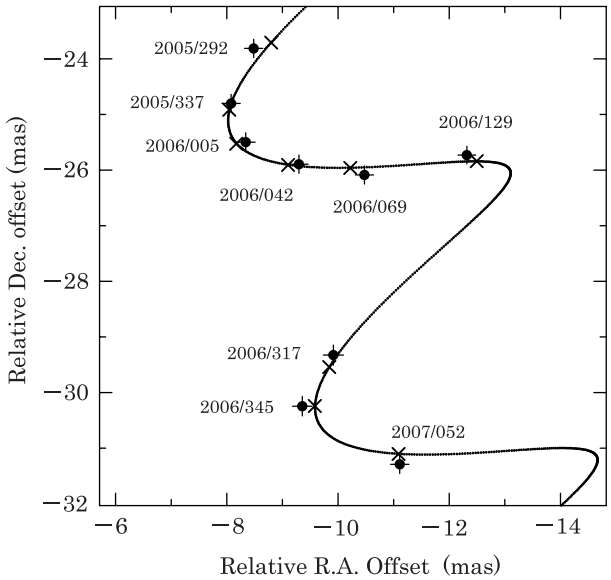

Fig. 3. Absolute positions of the reference maser spot in S Crt. Filled circles indicate the present results with error bars, and crosses indicate predicted positions. The solid curve indicates the combined motion of the best-fit results of the parallax and the proper motion. The axes indicate the position offsets with respect to the phase tracking center.

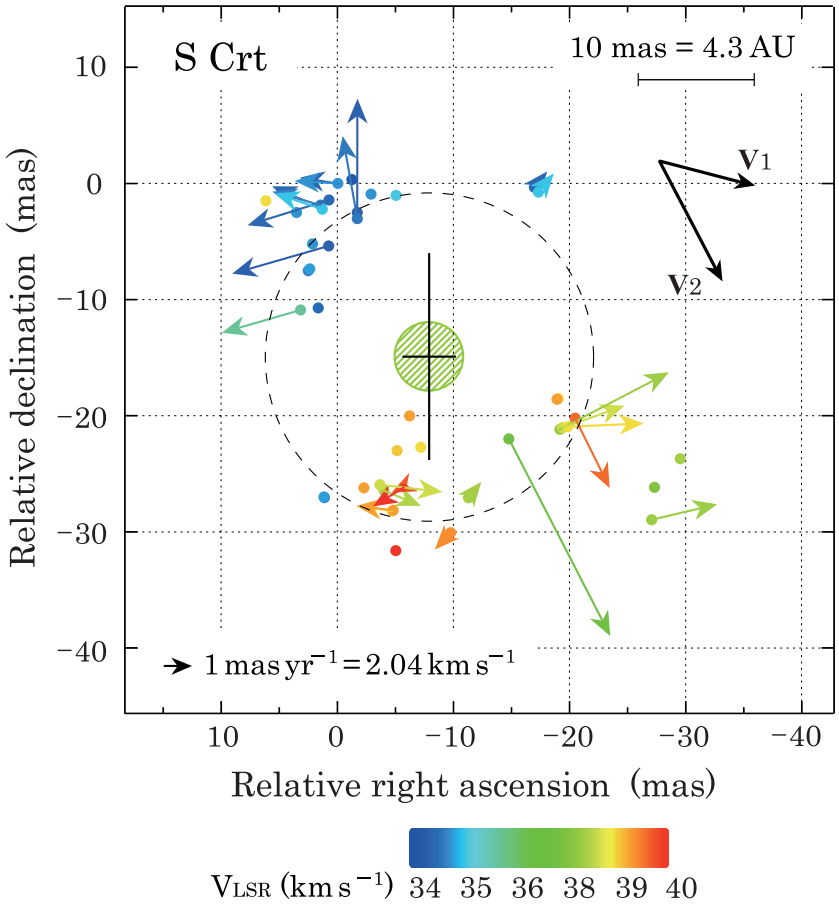

Fig. 4. Angular distribution and internal motion vectors of maser spots in S Crt. The spot color indicates the LSR velocity (see color index at the bottom). The stellar velocity of S Crt is 37.85 km s^{-1}. The arrow at the bottom-left corner indicates a proper motion of 1 mas yr^{-1}, corresponding to 2.04 km s^{-1} at the distance of 430 pc. The shaded-circle indicates the size of the stellar photosphere. The dashed line represents a circular fit to the maser distribution, and has a radius of 14.2 mas (see subsection 4.2 for details). The cross indicates the estimated stellar position. The bold arrows $\boldsymbol{V}_1$ and $\boldsymbol{V}_2$ are the eigenvectors for the largest eigenvalue indicating the major axes of maser distribution.

The reference source J1147−0724 exhibited an unresolved structure. The correlated amplitude as a function of (u, v) distance is flat, and the upper limit of the source size is 0.8 mas (FWHM), which is the minor axis of the synthesized beam in the present observation. In addition, we confirmed that the images of J1147−0724 showed no distinctive change during the observations.

3.2. *Maser Distribution and Internal Motions*

In figure 4, we present the angular distribution and three-dimensional velocity field of maser spots in S Crt covering a 60 mas × 60 mas region. The maser spot with an LSR velocity of 34.7 km s^{-1} is placed at the map origin. At a distance of 430 pc, 1 mas corresponds to 0.43 AU, and 1 mas yr^{-1} corresponds to a velocity of 2.04 km s^{-1}. The color index in figure 4 shows the LSR velocity range from 34.0 to 41.0 km s^{-1}. The blue- and red-shifted components are separated into the north-east and southwest parts of the area. The relative motion of each spot (v_x, v_y) with respect to the reference spot are used to determine the average motion $(\bar{v_x}, \bar{v_y})$, and hence we obtained $(\bar{v_x}, \bar{v_y}) = (-1.605\,\mathrm{mas\,yr^{-1}}, -0.252\,\mathrm{mas\,yr^{-1}})$. We then subtracted $(\bar{v_x}, \bar{v_y})$ from (v_x, v_y) to obtain the internal motions (V_x, V_y), which are presented by the arrows in figure 4. We successfully detected the internal motions of 26 maser spots. The typical transverse speed was obtained to be 2.72 mas yr^{-1}, corresponding to 5.56 km s^{-1}, by averaging the internal motions of all 26 spots. The parameters of the motions are presented in table 2 in the increasing order of the LSR velocity.

For the reference spot, we subtracted the internal motion from the proper motion (μ_X, μ_Y), and thus, the proper motion of the S Crt system was estimated to be $(-3.17 \pm 0.22\,\mathrm{mas\,yr^{-1}}, -5.41 \pm 0.22\,\mathrm{mas\,yr^{-1}})$. In the new HIPPARCOS catalog (van Leeuwen 2007), the absolute proper motion of S Crt was $(-3.37 \pm 1.00\,\mathrm{mas\,yr^{-1}}, -4.67 \pm 0.75\,\mathrm{mas\,yr^{-1}})$, representing good consistency with our result within the errors.

4. Discussion

4.1. *Errors in the Positions*

Since it is difficult to identify contributions to the positional errors in individual VLBI observations (Kurayama et al. 2005; Hachisuka et al. 2006; Honma et al. 2007; Sato et al. 2007; Hirota et al. 2007; Imai et al. 2007), we applied errors

Table 2. Parameters of the detected maser spots.

ID	$V_{\rm LSR}$ (km s^{-1})	X (mas)	Y (mas)	S (Jy beam^{-1})	V_x (mas yr^{-1})	σ_{Vx}	V_y (mas yr^{-1})	σ_{Vy}
1	34.10	−1.25	0.34	2.3	...	...	...	...
2	34.53	−1.71	−2.50	2.7	−0.01	0.01	4.90	2.58
3	34.55	0.76	−5.39	4.4	4.15	0.55	−1.19	0.06
4	34.68	0.00	0.00	19.5	1.61	...	0.25	...
5	34.68	−16.97	−0.34	4.6	−0.55	0.02	0.69	0.09
6	34.68	−2.85	−0.91	8.1	...	...	...	...
7	34.72	0.73	−1.42	1.8	3.50	0.29	−1.09	0.45
8	34.72	1.43	−2.00	1.9	2.10	0.54	0.88	0.14
9	34.74	1.64	−10.71	5.8	...	...	...	...
10	34.94	−1.72	−3.04	1.6	0.63	0.50	3.56	0.37
11	34.95	1.45	−1.86	35.4	2.08	0.89	0.58	0.06
12	34.97	2.51	−7.51	2.3	...	...	...	...
13	34.97	1.11	−27.05	2.5	...	...	...	...
14	35.10	−0.03	0.01	8.4	1.85	0.74	0.10	0.04
15	35.10	−2.89	−0.92	4.9	...	...	...	...
16	35.16	3.52	−2.50	3.5	...	...	...	...
17	35.16	2.13	−5.20	3.2	...	...	...	...
18	35.18	2.38	−7.37	2.1	...	...	...	...
19	35.18	1.14	−27.01	2.1	...	...	...	...
20	35.52	1.30	−2.21	1.5	2.05	0.90	0.68	0.36
21	35.52	−17.32	−0.74	1.3	−0.66	0.06	0.80	0.11
22	35.54	−5.04	−1.04	0.9	...	...	...	...
23	36.45	3.17	−10.90	1.3	3.39	0.52	−0.98	0.49
24	37.89	−14.77	−22.00	0.8	−4.37	0	−8.49	0
25	38.32	−27.32	−26.17	1.3	...	...	...	...
26	38.73	−27.06	−28.97	1.0	−2.83	0.15	0.67	0.45
27	38.73	−19.16	−21.19	0.9	−4.70	0	2.46	0
28	38.74	−29.53	−23.72	0.9	...	...	...	...
29	38.74	−11.30	−27.07	1.0	−0.55	0.02	0.69	0.09
30	38.91	−4.01	−26.46	1.1	−1.60	0.43	−0.65	0.29
31	39.15	−3.67	−25.96	0.8	−2.69	0.30	−0.30	0.18
32	39.15	−19.40	−21.04	2.2	−2.67	0.37	0.95	0.44
33	39.57	−19.87	−20.95	3.4	−3.26	0	0.14	0
34	39.57	−7.18	−22.73	2.2	...	...	...	...
35	39.57	−19.02	−18.52	2.0	...	...	...	...
36	39.59	6.15	−1.49	1.8	...	...	...	...
37	39.61	−4.73	−28.23	0.7	1.49	0	0.23	0
38	39.74	−5.14	−23.02	1.0	...	...	...	...
39	40.00	−18.91	−18.58	1.2	...	...	...	...
40	40.01	−6.22	−20.02	4.7	...	...	...	...
41	40.03	−4.81	−28.14	1.0	1.59	0	0.18	0
42	40.03	−2.29	−26.22	2.0	...	...	...	...
43	40.16	−9.75	−30.09	1.6	0.68	0.38	−0.72	0.06
44	40.42	−20.47	−20.21	1.1	−1.49	0.23	−3.01	0.51
45	40.58	−5.73	−26.12	2.6	0.54	0.05	−0.26	0.17
46	41.00	−5.03	−31.63	1.1	...	...	...	...
47	41.00	−5.70	−26.20	5.4	1.32	1.27	−0.81	0.42

Column (1) — Component ID. Column (2) — LSR velocity in km s^{-1}. Column (3) — offset positions in RA relative to the original phase center. Column (4) — offset positions in Dec relative to the original phase center. Column (5) — brightness of the spot at the first detection in Jy beam^{-1}. Column (6) — best fit linear motion in RA in mas yr^{-1}. Column (7) — standard errors of the motions in RA. In case the number of successful detections were restricted to be only twice, we adopted the standard errors σ_X and σ_Y for the spot as zero. Column (8) — best fit linear motion in Dec in mas yr^{-1}. Column (9) — standard errors of the motions in Dec.

in each observation by evaluating the following three error sources: (1) a zenith atmospheric delay offset at each station, (2) station position errors, and (3) image quality. The best estimates of the zenith atmospheric delay offsets fell within the range of ± 3 cm. Errors in the a priori station positions can result in additional phase residuals. Therefore, we assumed an offset of 3 cm, even after an atmospheric offset calibration was made.

For a given separation of the zenith angles between two sources, ΔZ, the difference of the signal path lengths, Δl, between the two directions caused by the zenith atmospheric delay residual, l_0, can be estimated as

$$\Delta l = l_0 \Delta Z \frac{d}{dZ}\left(\frac{1}{\cos Z}\right), \quad (1)$$

where Z is the mean zenith angle of the observed sources. We adopted $1\overset{\circ}{.}23$ as an approximation of ΔZ. During our observations, the elevation angles higher than 30° were dominant. We assumed $Z = 50°$ as the zenith angle for estimating the errors of the worst case, and obtained $\Delta l = 0.12$ cm. Using a root sum squares of the major and minor axes of the synthesized beam ($\theta_{\rm b} = 1.7$ mas), we estimated a positional error of $\sigma_Z = 156\,\mu$as from the following expression:

$$\sigma_Z = \theta_{\rm b} \times \frac{\Delta l}{\lambda_{\rm H_2O}}, \quad (2)$$

where $\lambda_{\rm H_2O}$ is the wavelength corresponding to the rest frequency of water masers. Since the position accuracy of antennas were determined to be ~ 3 mm, based on geodetic observations at the S and X bands, we estimated the positional error (σ_D) attributed to the baseline errors to be $5\,\mu$as using the following expression:

$$\sigma_D = \sin\theta_{\rm SA} \times \frac{3\,{\rm mm}}{\lambda_{\rm H_2O}}, \quad (3)$$

where $\theta_{\rm SA} = 1\overset{\circ}{.}23$ is the separation angle of the source pair. In addition, we estimated the measurement error ($\sigma_I = \theta_{\rm b}/{\rm SNR}$, SNR is the signal-to-noise ratio), which depends on the SNRs of the phase-referenced images. Finally, we obtained the position errors of each phase-referenced image by adding up quadratically the error factors (σ_Z, σ_D, and σ_I). The error bars in figure 3 represent the errors in each observation; the averaged value of the errors is $167\,\mu$as.

4.2. *Maser Morphology*

Figure 4 shows the internal motions of the maser spots around S Crt found in the present observations. Since the maser spots show a bimodal distribution about radial velocities and positions, we extracted the kinematic essentials. The analytic tools based on the diagonalization of the velocity variance–covariance matrix (VVCM) (Bloemhof 2000) and position variance–covariance matrix were used.

The elements of the VVCM matrix are presented as

$$\sigma_{jk} = \frac{1}{N-1}\sum_{i=1}^{N}(V_{j,i} - \bar{V_j})(V_{k,i} - \bar{V_k}), \quad (4)$$

where the diagonal elements are the velocity dispersion. Here, j and k denote three orthogonal space axes (e.g., RA, Dec, and radial coordinate z), i denotes the ith maser spot in a collection totalling N (= 26), and the bar indicates averaging over the maser spots.

The vector $\boldsymbol{V}_1$ (figure 4), which is a two-dimensional projection of the eigenvector for the largest eigenvalue, is the major principal axis of the VVCM. This axis of the maximum internal velocity dispersion is the outflow axis. The axis of $\boldsymbol{V}_1$ lies at a P.A. of $\sim 255°$, and also makes an inclination angle of $\sim 43°$ with the plane of the sky, with the southwest lobe directed into the page (away from the observer). The VVCM was initially evaluated in a coordinate system with axes RA, Dec, and the radial coordinate z increasing toward the source, and then it was diagonalized.

We also considered the two-dimensional variance–covariance matrix to quantify the angular distribution of the maser spots. Here, the number of maser spots is 26, the same as in the case of VVCM. In diagonalization of this matrix, one eigenvalue larger than the other by a factor of 3.1 was obtained. The corresponding eigenvector $\boldsymbol{V}_2$ presented in figure 4 indicates the spatial elongation of the maser distribution. The position angle of this axis was found to be $\sim 208°$. Although the maser velocity and the position axes show a discrepancy of $\sim 47°$, the directions of these model-independent axes indicate the bipolar outflow with the major axis along northeast–southwest. This dynamical property was not revealed by previous observations (Bowers & Johnston 1994).

We estimated the stellar position from the present result by using kinematic information. Since the motion of each maser spot is powered by the forming star, its position can be estimated as the origin of these motions. Here, we take one of the simplest kinematic models, which assumes a linear motion with a constant velocity from a single origin. This technique is essentially the same as that used in Imai et al. (2000) and Honma et al. (2007). Based on this modeling, we obtained the origin of the maser motions that most effectively explain the observed positions and velocities. The stellar position from this kinematic analysis, the kinematic center was obtained to be $(X, Y) = (-7.9 \pm 1.8\,{\rm mas}, -14.9 \pm 13.3\,{\rm mas})$, which is indicated by the cross with error bars in figure 4. We used the first-order moment with respect to the determined stellar position in order to find a typical distance of maser spots. The obtained distance was 14.2 ± 3.5 mas, which is presented with the dashed line in figure 4. At a distance of 430 pc, the corresponding linear length is 6.11 AU. Since we estimated the inclination angle of the outflow axis, this projected length can be converted to a linear radius of 8.96 AU.

Nineteen years ago, the angular distribution of the masers was firstly observed with the NRAO Very Large Array in its A configuration (Bowers & Johnston 1994). The masers were uniformly distributed over a 40 mas × 40 mas region with the LSR velocities ranging evenly from 33.4 to 44.2 km s^{-1} (figure 13 of Bowers and Johnston 1994). In their study, the blue-(red-)shifted spots were found northeast (southwest) of the maser region. In addition, masers with intermediate velocities were found in the central region. Although the extent of the distribution is consistent with our result, we did not detect the masers in the central region. In figure 4, the maser spots are mainly found at the peripheral region of the distribution. During the period of 2006.3–2007.0, we could not find

emission with intermediate velocities (see figure 1b), which can explain the absence of intermediate velocity maser spots. On the other hand, at the beginning and end of our VLBI observations, the masers with intermediate velocities were found in the total power spectrum, which were distributed in the peripheral region. Since Bowers and Johnston (1994) did not precisely mention the flux densities and the sizes of each spot, it is difficult to specify the reason for our non-detection of the masers in the central region. However, we can speculate the reason: (1) Our image sensitivities were not high enough to detect them. The rms noise 38 mJy beam^{-1} of Bowers and Johnston (1994) was lower than that of the present VLBI observations, 90 mJy beam^{-1}. (2) The masers in the central region had faded before the present VLBI observations. (3) The masers were extended and diffuse, and therefore they were resolved out with the synthesized beam of VERA. For example, we found the effect of resolve-out (e.g., $\leq 30\%$ in 2006 March) from a comparison between the cross-power spectrum (figure 2) and the total-power spectrum (figure 1b).

4.3. Stellar Diameter and Temperature

We extracted the stellar properties of S Crt using the distance. Aringer et al. (1999) determined the temperature of the photosphere ($T_{\rm BB}$) in S Crt to be 3097 ± 100 K by fitting two blackbodies to its infrared spectrum. Using this temperature, we estimated an acceptable temperature range of 2600–3500 K. Here, we assumed that the light variation of 0.8 mag (figure 1a) is the same in the infrared, and is caused only by the temperature variation. Aringer et al. (1999) reported that Mira variables show $T_{\rm BB} = 2418$–2902 K and semiregular variables show $T_{\rm BB} = 3005$–3500 K. The estimated temperature range of S Crt is consistent with their finding.

It is worthwhile estimating the stellar radius of S Crt, since there has been no direct measurement. Using the apparent magnitudes in the infrared (J, H, and K), $T_{\rm BB}$ (3097 K), and the distance (430 pc), we estimated the radius of the S Crt photosphere (R_*) to be $(1.81 \pm 0.14) \times 10^{13}$ cm ($260 \pm 20\ R_\odot$). This is presented with a shaded-circle in figure 4, and the center of the circle is placed at the kinematic center. Using this radius, we estimated an acceptable radius range of 213–309 $R_\odot$, under the assumption that the light variation is caused, now, only by the radius variation. In the studies of Haniff, Scholz, and Tuthill (1995) and van Leeuwen et al. (1997), the R_*s of a dozen Mira variables were presented, and most $R_*/R_\odot$ values were found to be larger than 300. The photospheric radius of S Crt is close to the lower limits to those of the Mira variables given in the literature. Since estimates of R_* and $T_{\rm BB}$ are now available, the luminosity (L_*) of S Crt is estimated to be 2.29×10^{30} (W), resulting in a $L_*/L_\odot$ ratio of 5970.

A similar analysis of data for a larger number of Mira and semiregular variables would be very useful for a better understanding of the difference and similarities between Mira variables and semiregular varialiles.

5. Summary

We have used VLBI monitoring observations with VERA to measure the absolute proper motions of a maser spot in S Crt with respect to the quasar J1147−0724. We obtained an annual parallax of 2.33 ± 0.13 mas, corresponding to a distance of 430^{+25}_{-23} pc.

Nearly two years astrometric observations revealed the internal motions of 26 maser spots for the first time. Taking into account the internal motions of the reference maser spot, the absolute proper motion of the S Crt system was obtained to be (-3.17 ± 0.22 mas yr^{-1}, -5.41 ± 0.22 mas yr^{-1}), which is consistent with the result in the new HIPPARCOS catalog.

The three-dimensional velocity field of the maser spots in S Crt was also detected, clearly outlining a bipolar outflow with the major axis along northeast–southwest. The inclination of the axis with respect to the sky plane was $\sim 43°$. The angular size of the maser distribution can be converted to a linear maser distribution radius of 8.96 AU.

Using a photospheric temperature of 3097 K (Aringer et al. 1999), the K band apparent magnitude, $m_K = 0.79$, and the distance of 430 pc, the linear radius of the S Crt photosphere (R_*) was estimated to be $(1.81 \pm 0.14) \times 10^{13}$ cm ($260 \pm 20\ R_\odot$). This radius is comparable with the lower limits to those of Mira variables in the literature.

References

Antipin, S. V., Pastukhova, E. N., & Samus, N. N. 2005, Inf. Bull. Variable Stars, 5613, 1

Aringer, B., Höfner, S., Wiedemann, G., Hron, J., Jørgensen, U. G., Käufl, H. U., & Windsteig, W. 1999, A&A, 342, 799

Benson, P. J., Little-Marenin, I. R., Woods, T. C., Attridge, J. M., Blais, K. A., Rudolph, D. B., Rubiera, M. E., & Keefe, H. L. 1990, ApJS, 74, 911

Bloemhof, E. E. 2000, ApJ, 533, 893

Bowers, P. F., & Johnston, K. J. 1994, ApJS, 92, 189

Hachisuka, K., et al. 2006, ApJ, 645, 337

Haniff, C. A., Scholz, M., & Tuthill, P. G. 1995, MNRAS, 276, 640

Hirota, T., et al. 2007, PASJ, 59, 897

Hirota, T., et al. 2008, PASJ, 60, 37

Honma, M., et al. 2007, PASJ, 59, 889

Imai, H., et al. 2007, PASJ, 59, 1107

Imai, H., Kameya, O., Sasao, T., Miyoshi, M., Deguchi, S., Horiuchi, S., & Asaki, Y. 2000, ApJ, 538, 751

Jike, T., Fukuzaki, Y., Shibuya, K., Doi, K., Manabe, S., Jauncey, D. L. Nicolson, G. D., & McCulloch, P. M. 2005, Polar Geoscience, 18, 26

Kawaguchi, N., Sasao, T., & Manabe, S. 2000, Proc. SPIE, 4015, 544

Kobayashi, H., et al. 2003, ASP Conf. Ser., 306, 48

Kurayama, T., Sasao, T., & Kobayashi, H. 2005, ApJ, 627, L49

Ma, C., et al. 1998, AJ, 116, 516

Manabe, S., Yokoyama, K., & Sakai, S. 1991, IERS Techn. Note, 8, 61

Patel, N. A., Joseph, A., & Ganesan, R. 1992, JA&A, 13, 241

Perryman, M. A. C., et al. 1997, A&A, 323, L49

Petrov, L., Hirota, T., Honma, M., Shibata, K. M., Jike, T., & Kobayashi, H. 2007, AJ, 133, 2487

Pojmański, G. 1997, Acta Astronomica, 47, 467

Sato, M., et al. 2007, PASJ, 59, 743
Shibata, K. M., Kameno, S., Inoue, M., & Kobayashi, H. 1998, in ASP Conf. Ser. 144, IAU Colloq. 164, Radio Emission from Galactic and Extragalactic Compact Sources, ed. J. A. Zensus, G. B. Taylor, & J. M. Wrobel (San Francisco: ASP), 413
Shimoikura, T., Kobayashi, H., Omodaka, T., Diamond, P. J., Matveyenko, L. I., & Fujisawa, K. 2005, ApJ, 634, 459
Shintani, M., et al. 2008, PASJ, 60, 1077
van Leeuwen, F. 2007, Hipparcos, the New Reduction of the Raw Data. Series: Astrophysics and Space Science Library v. 350 (Dordrecht: Springer)
van Leeuwen, F., Feast, M. W., Whitelock, P. A., & Yudin, B. 1997, MNRAS, 287, 955
Vlemmings, W. H. T., van Langevelde, H. J., Diamond, P. J., Habing, H. J., & Schilizzi, R. T. 2003, A&A, 407, 213
Whitelock, P. A., Feast, M. W., & van Leeuwen, F. 2008, MNRAS, 386, 313